Supporting Information for

Valence Tautomerism in Chromium Half-Sandwich Triarylmethylium Dyads

Anja Rehse, Michael Linseis, Mykhailo Azarkh, Malte Drescher and Rainer F. Winter *

Department of Chemistry, Universität Konstanz, Universitätsstraße 10, 78464 Konstanz, Germany
* Correspondence: rainer.winter@uni-konstanz.de

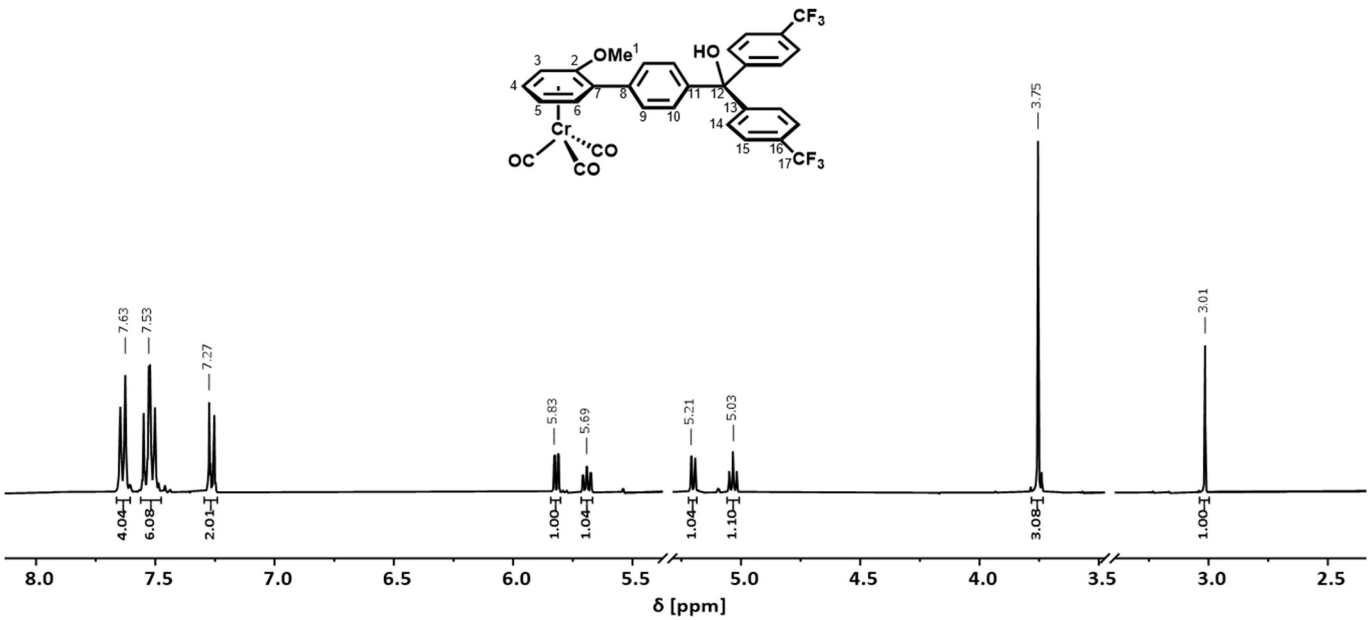


Figure S1. ^{1}H-NMR spectrum of complex **1-OH** (400 MHz, CD_2Cl_2).

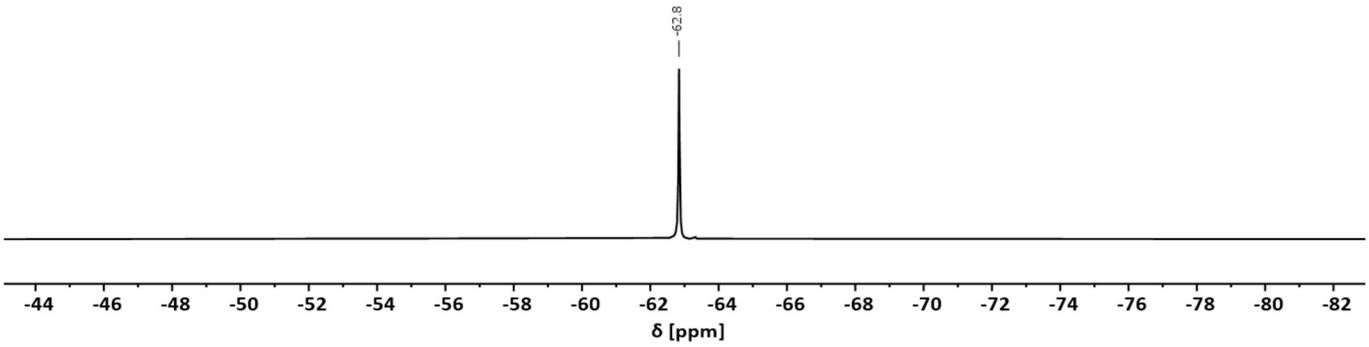


Figure S2. ^{19}F{^{1}H}-NMR spectrum of complex **1-OH** (376 MHz, CD_2Cl_2).

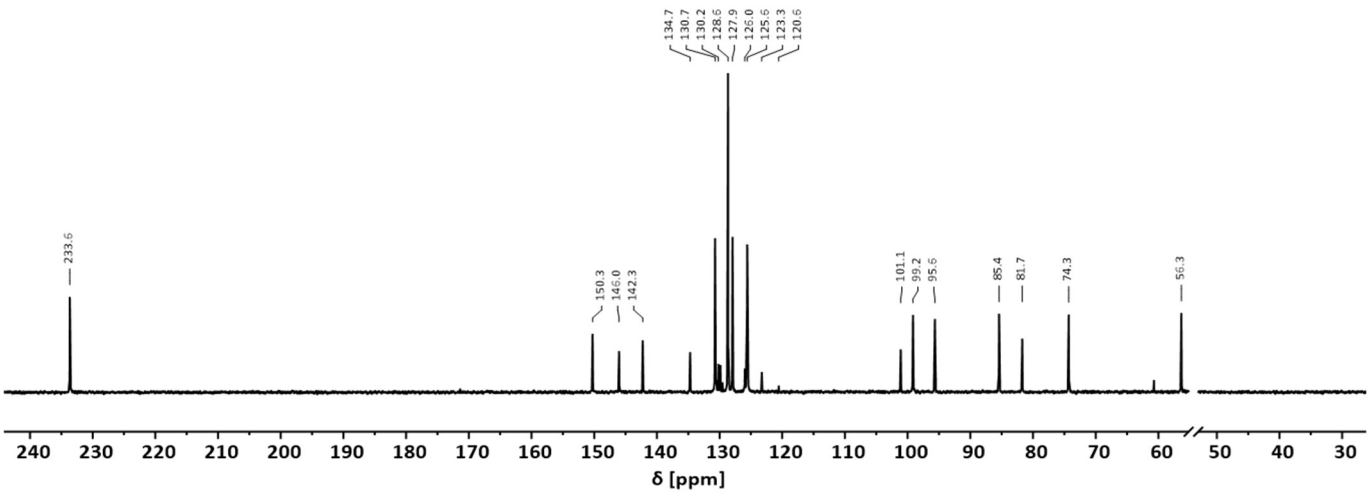


Figure S3. ^{13}C{^{1}H}-NMR spectrum of complex **1-OH** (101 MHz, CD_2Cl_2).

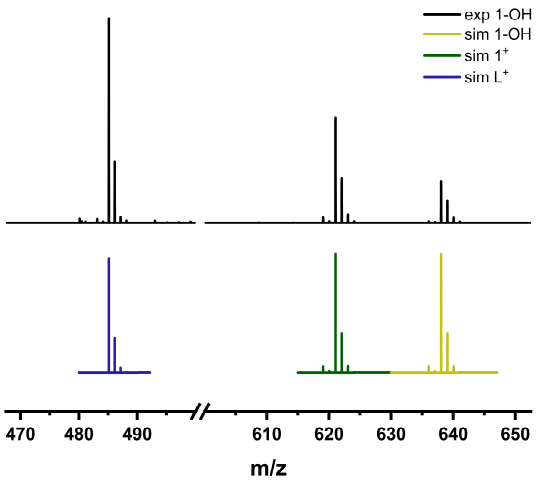


Figure S4. Experimental (black) and simulated (carbinol yellow, tritylium complex green, tritylium ligand blue) mass spectrum of complex **1-OH**.

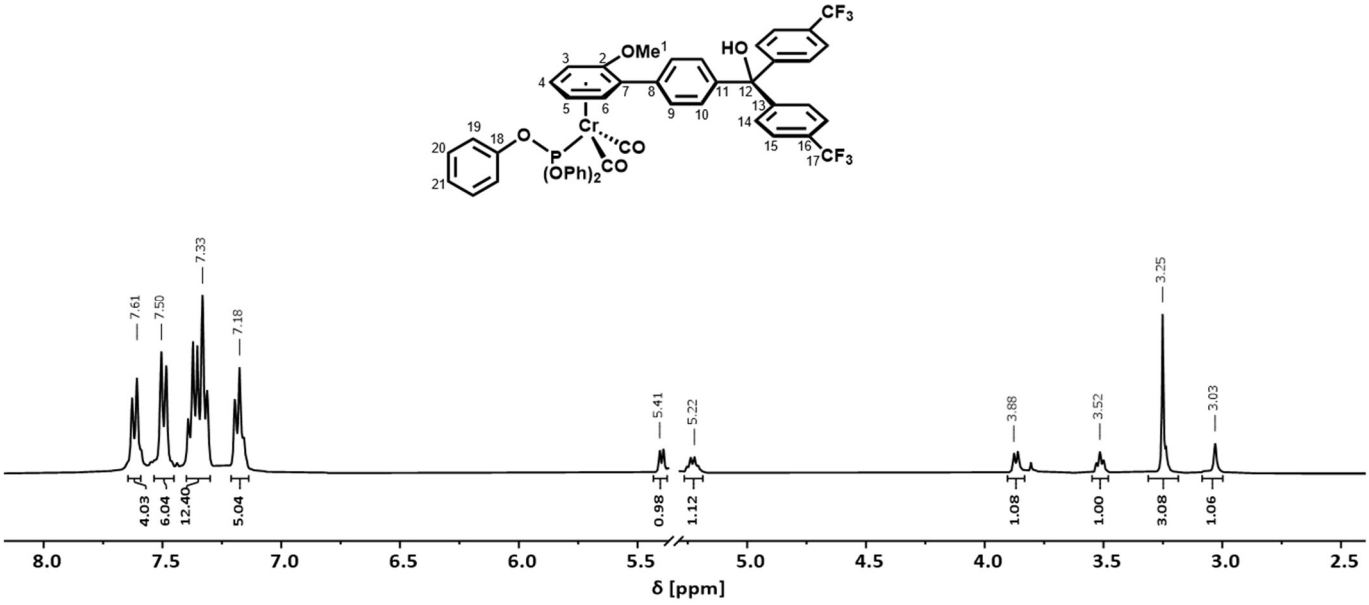


Figure S5. ^{1}H-NMR spectrum of complex **2-OH** (400 MHz, CD_2Cl_2).

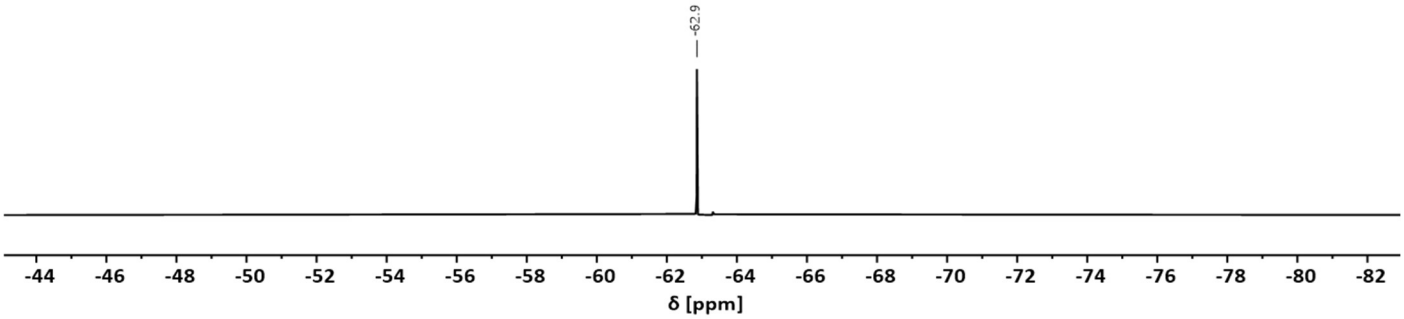


Figure S6. ^{19}F{^{1}H}-NMR spectrum of complex **2-OH** (376 MHz, CD_2Cl_2).

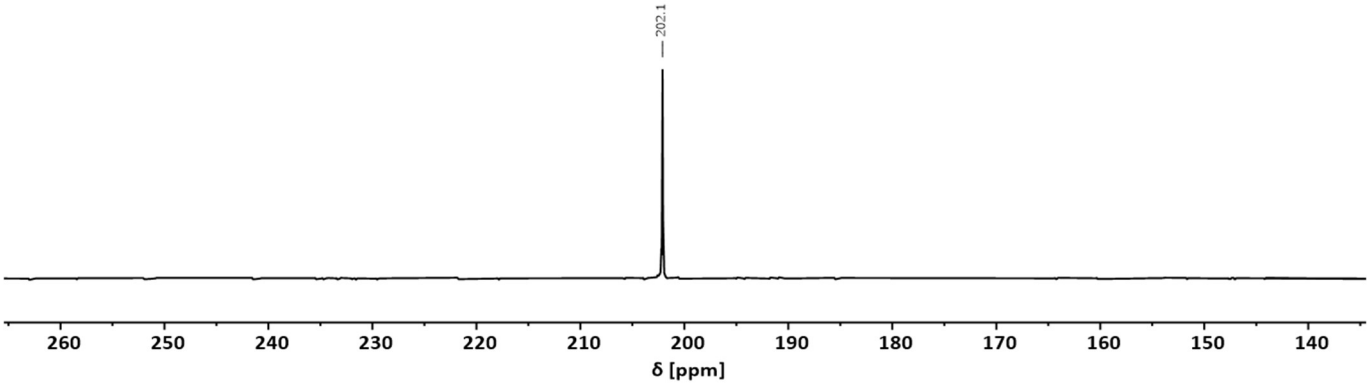


Figure S7. $^{31}P\{^{1}H\}$-NMR spectrum of complex **2-OH** (162 MHz, CD_2Cl_2).

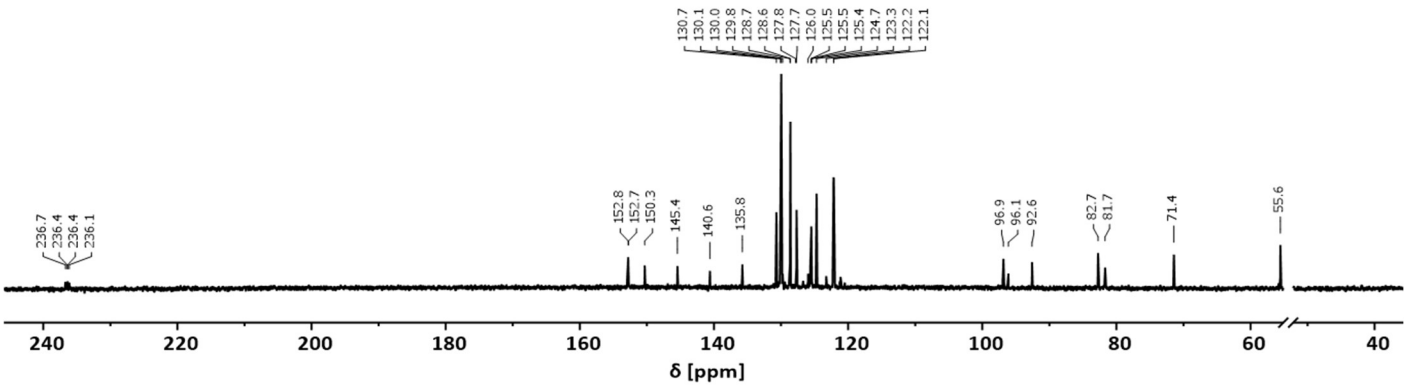


Figure S8. $^{13}C\{^{1}H\}$-NMR spectrum of complex **2-OH** (101 MHz, CD_2Cl_2).

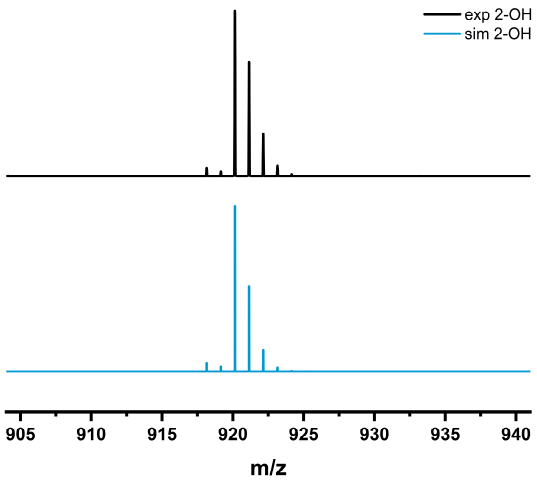


Figure S9. Experimental (black) and simulated (blue) mass spectrum of complex **2-OH**.

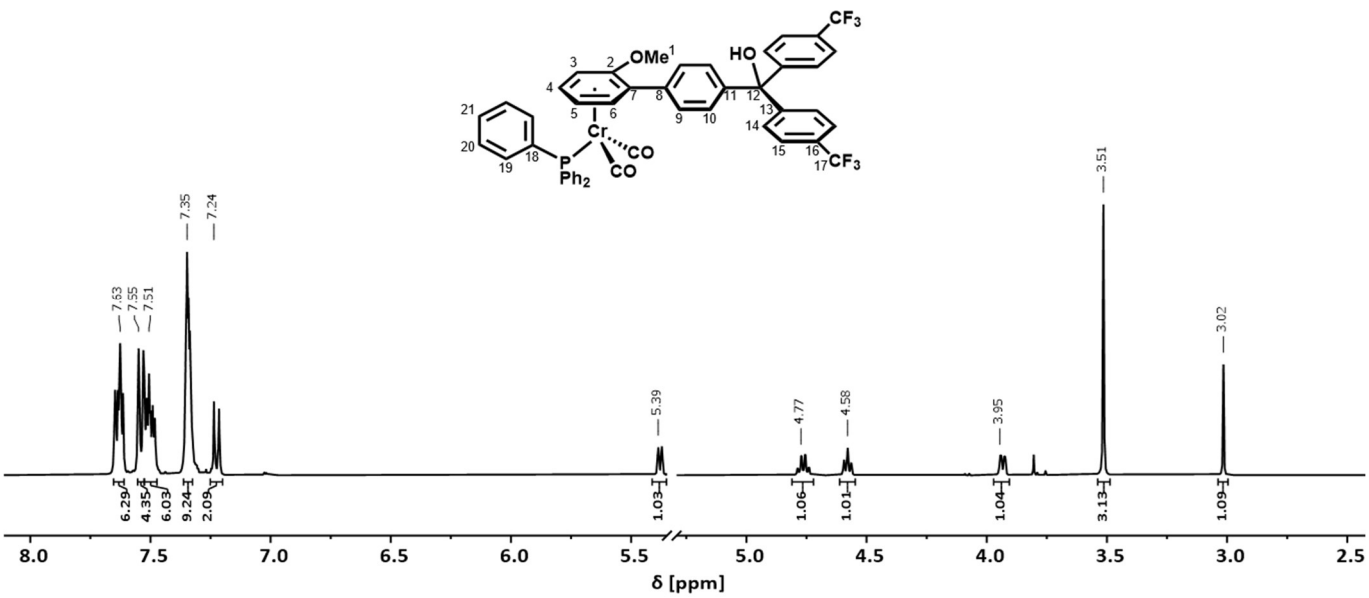


Figure S10. ^{1}H-NMR spectrum of complex **3-OH** (400 MHz, CD_2Cl_2).

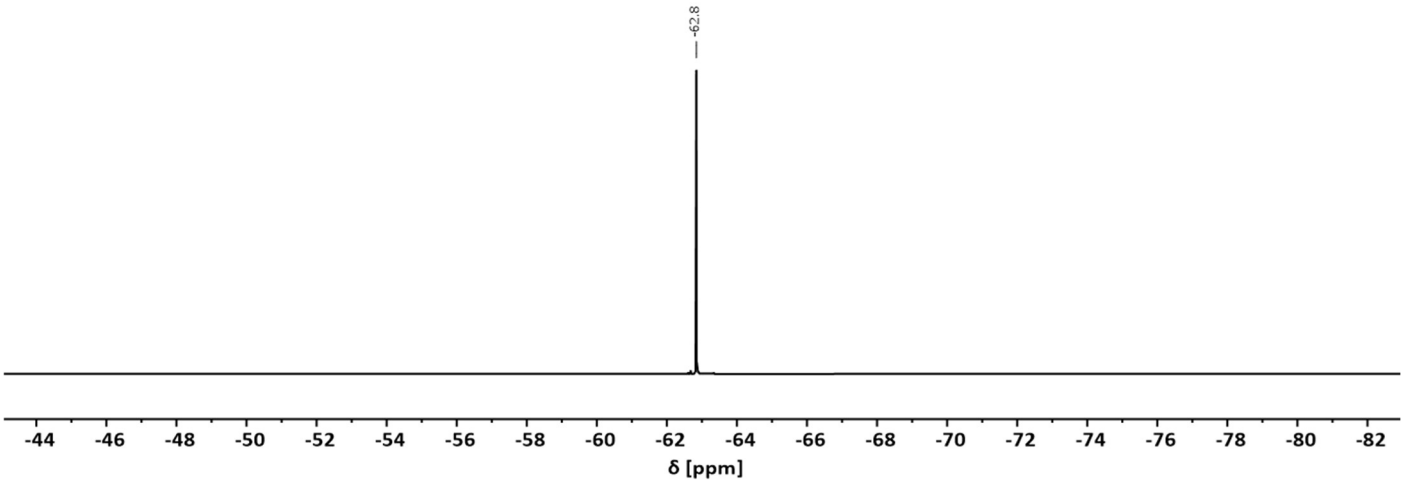


Figure S11. ^{19}F{^{1}H}-NMR spectrum of complex **3-OH** (376 MHz, CD_2Cl_2).

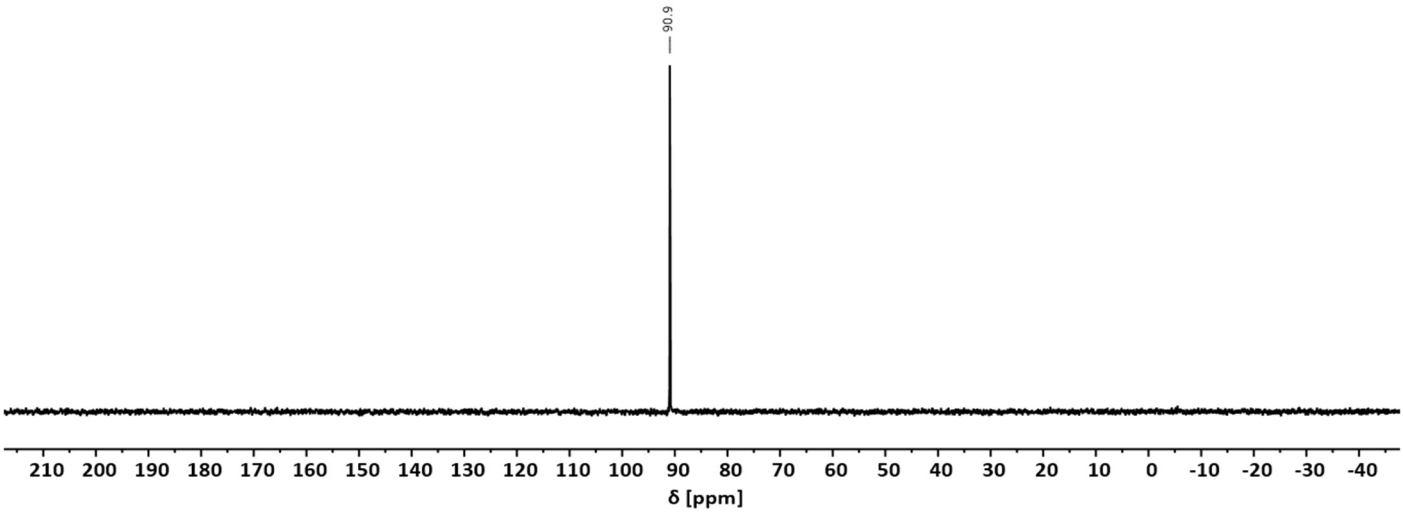


Figure S12. ^{31}P{^{1}H}-NMR spectrum of complex **3-OH** (162 MHz, CD_2Cl_2).

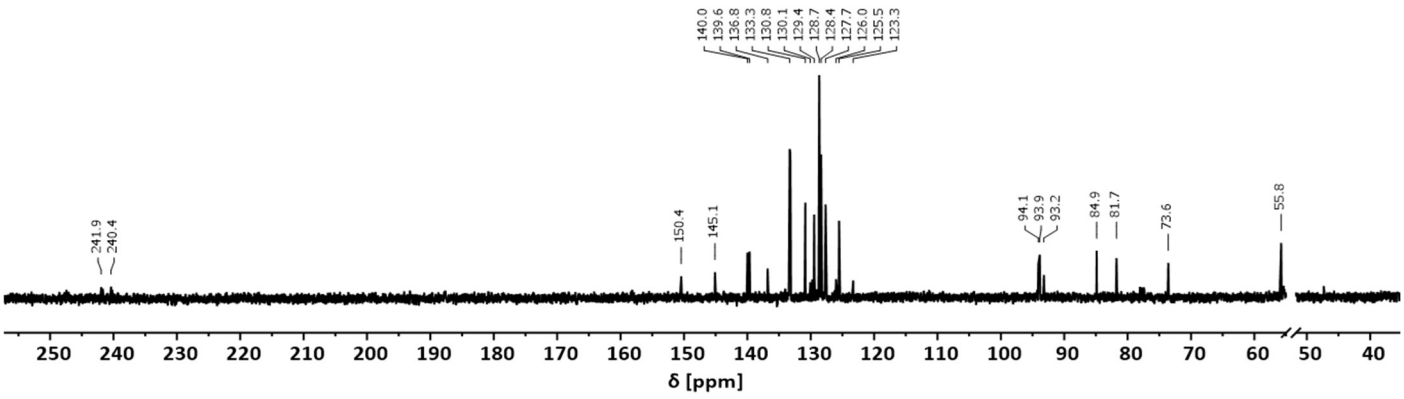


Figure S13. $^{13}C\{^{1}H\}$-NMR spectrum of complex **3-OH** (101 MHz, CD_2Cl_2).

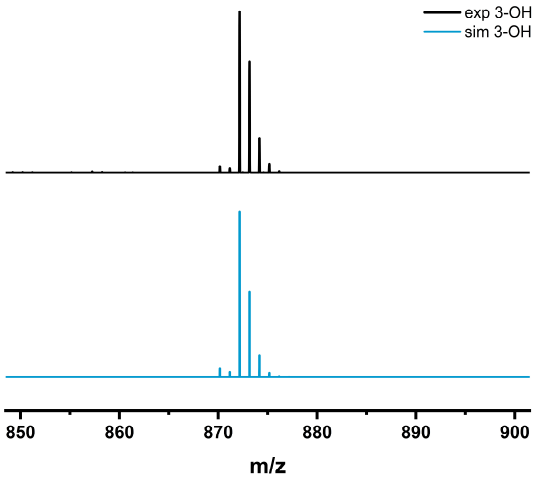


Figure S14. Experimental (black) and simulated (blue) mass spectrum of complex **3-OH**.

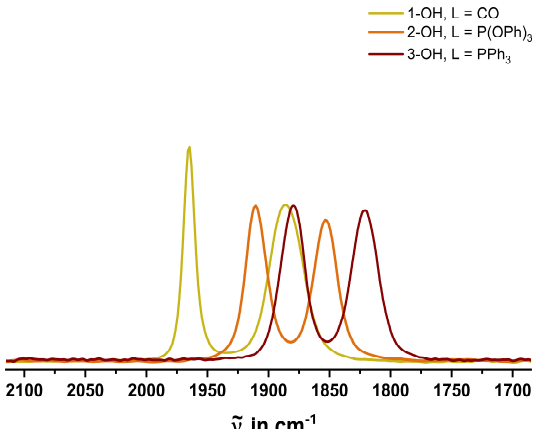


Figure S15. CO stretching vibrations in the IR spectra of complexes **1-OH** - **3-OH** in CH_2Cl_2.

Table S1. Crystal data and structure refinement for [(biaryl-ester)Cr(CO)$_3$] **1′**.

Empirical formula	$CrC_{18}O_6H_{14}$
Formula weight	378.29
Temperature / K	100
Crystal system	triclinic
Space group	*P*-1
a / Å	7.3806(8)
b / Å	9.6181(9)
c / Å	12.1058(12)
α / °	100.346(8)
β / °	105.803(8)
γ / °	92.640(8)
Volume / Å^3	809.33(15)
Z	2
ρ_{calc}g / cm^3	1.552
μ / mm^{-1}	0.739
F(000)	388.0
Crystal size / mm^3	0.2 × 0.2 × 0.2
Radiation	Mo Kα (λ = 0.71073)
2Θ range for data collection / °	5.766 to 55.196
Index ranges	$-9 \le h \le 9$, $-12 \le k \le 12$, $-15 \le l \le 15$
Reflections collected	9772
Independent reflections	3726 [R_{int} = 0.0413, R_{sigma} = 0.0331]
Data/restraints/parameters	3726/0/229
Goodness-of-fit on F^2	1.053
Final *R* indexes [$I \ge 2\sigma$ (I)]	R_1 = 0.0714, wR_2 = 0.1894
Final *R* indexes [all data]	R_1 = 0.0809, wR_2 = 0.2049
Largest diff. peak/hole / e Å^{-3}	1.86/-1.16

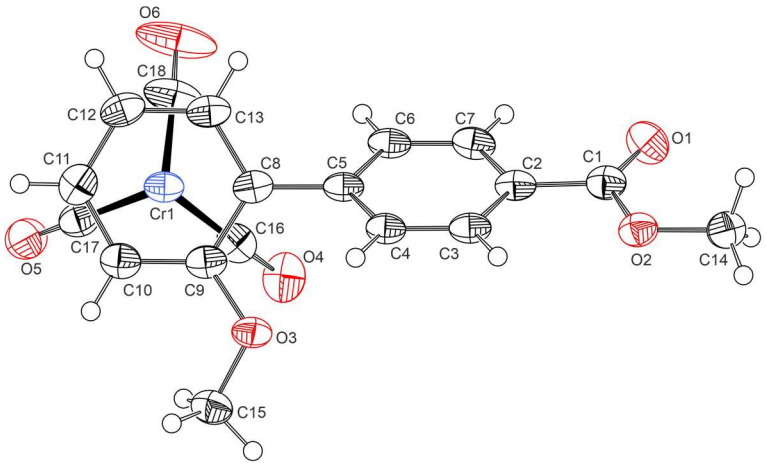


Figure S16. ORTEP of the S_p enantiomer of [(biaryl-ester)Cr(CO)$_3$], complex **1′**, with the atomic numbering. Ellipsoids are displayed at the 50% probability level.

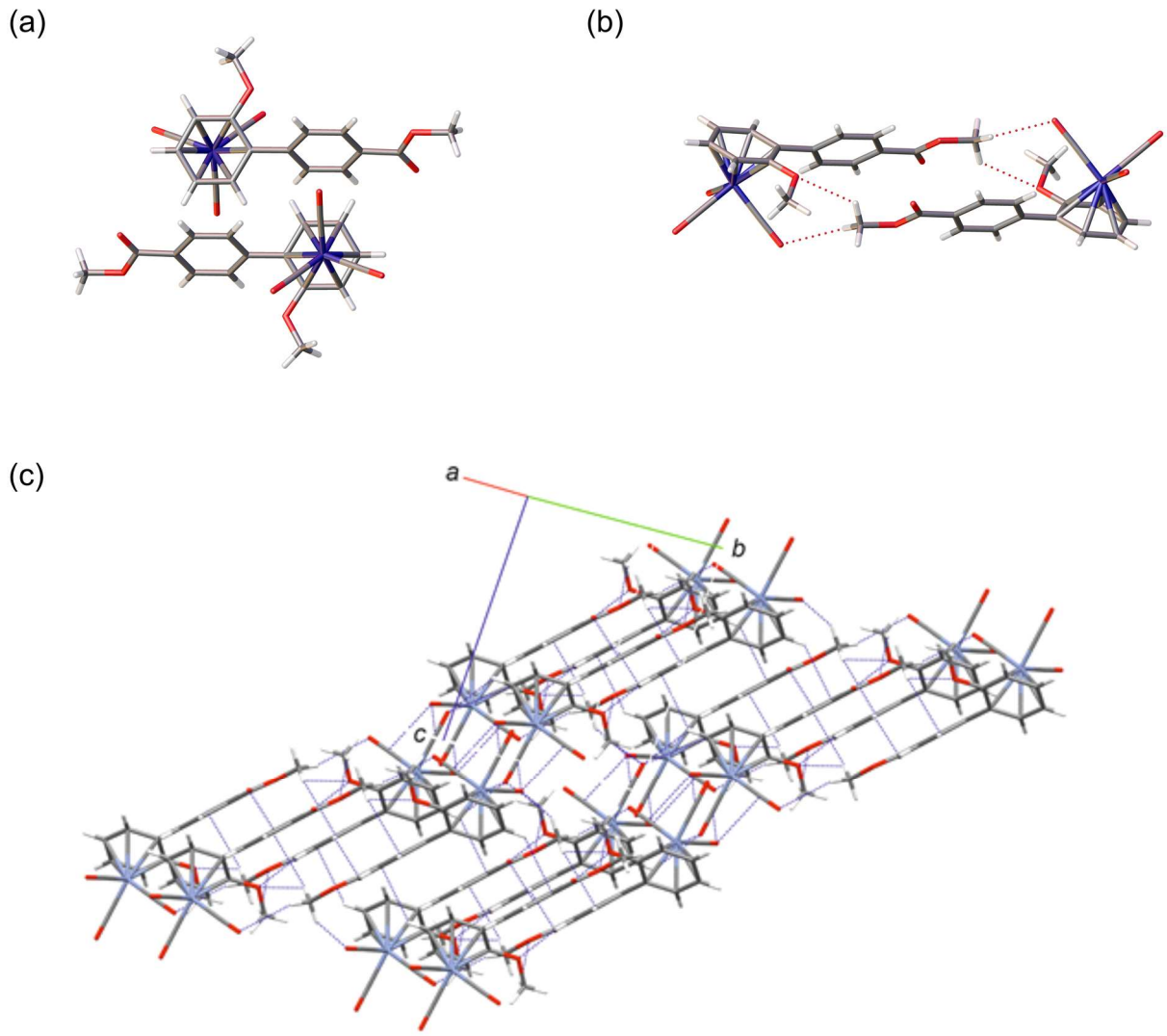


Figure S17. (a) The two enantiomers within the unit cell of **1′**. (b) Tail-to-tail dimers of **1′**. (c) Packing of **1′** in the crystal. Short contacts are indicated by blue and red broken lines, respectively.

Table S2. Crystal data and structure refinement for **3-OH**.

Empirical formula	$C_{56}H_{55}CrF_6O_6P$
Formula weight	1020.97
Temperature / K	100
Crystal system	monoclinic
Space group	$P2_1/c$
a / Å	20.7617(8)
b / Å	13.7170(3)
c / Å	17.9942(7)
α / °	90
β / °	101.005(3)
γ / °	90
Volume / Å^3	5030.3(3)
Z	4
ρ_{calc}g / cm^3	1.348
μ / mm^{-1}	0.332
F(000)	2128.0
Crystal size / mm^3	0.4 × 0.267 × 0.2
Radiation	Mo Kα (λ = 0.71073)
2Θ range for data collection / °	4.612 to 51.912
Index ranges	$-25 \le h \le 25$, $-16 \le k \le 16$, $-22 \le l \le 19$
Reflections collected	22453
Independent reflections	9749 [R_{int} = 0.0401, R_{sigma} = 0.0570]
Data/restraints/parameters	9749/185/791
Goodness-of-fit on F^2	1.033
Final R indexes [$I \ge 2\sigma$ (I)]	R_1 = 0.0566, wR_2 = 0.1327
Final R indexes [all data]	R_1 = 0.0974, wR_2 = 0.1538
Largest diff. peak/hole / e Å^{-3}	0.47/-0.54

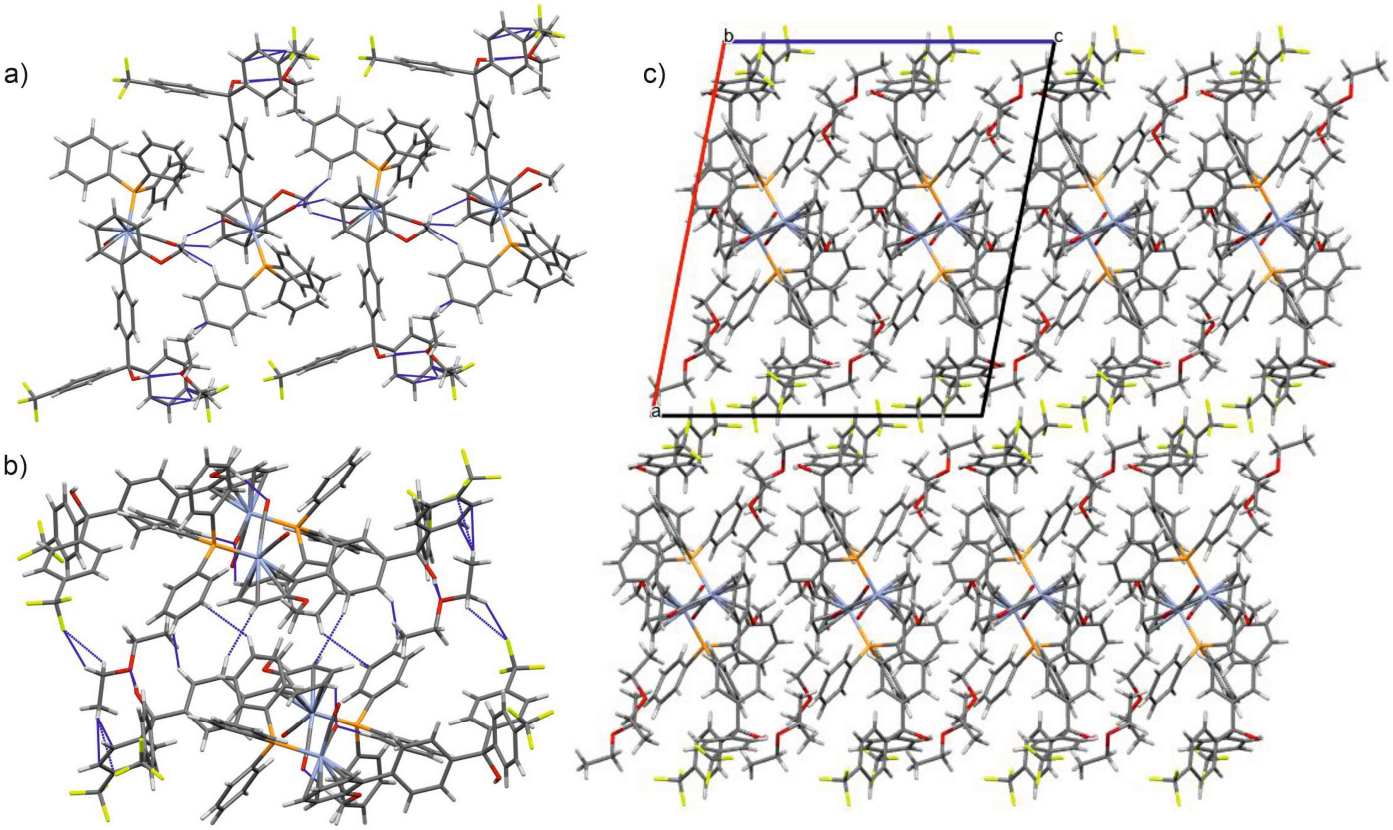


Figure S18. a) Chains of alternately aligned R_P/S_P enantiomers of **3-OH** with short intermolecular contacts indicated by blue broken lines progressing along the *b* axis of the unit cell. b) A view of two pairs of R_P/S_P enantiomers with the hydrogen-bonded ether solvent molecules. Short intermolecular contacts by C-H···π and C-H···F interactions are indicated by blue broken lines. c) Packing of the molecules within the unit cell as viewed along the *b* axis.

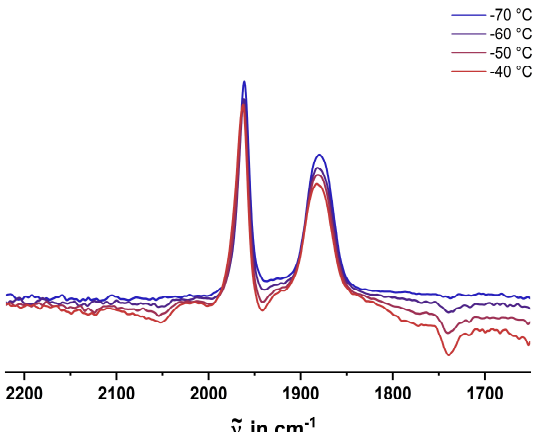


Figure S19. IR spectra of complex $\mathbf{1}^{+}$ in CH_2Cl_2 at temperatures between -70 and -40 °C.

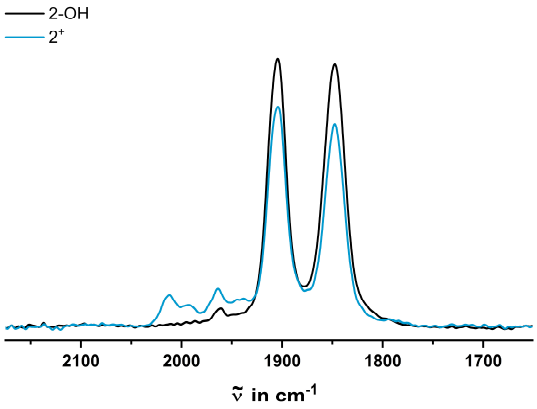


Figure S20. Basline-corrected IR spectra of **2-OH** and $\mathbf{2}^{+}$ in CH_2Cl_2 at -70 °C.

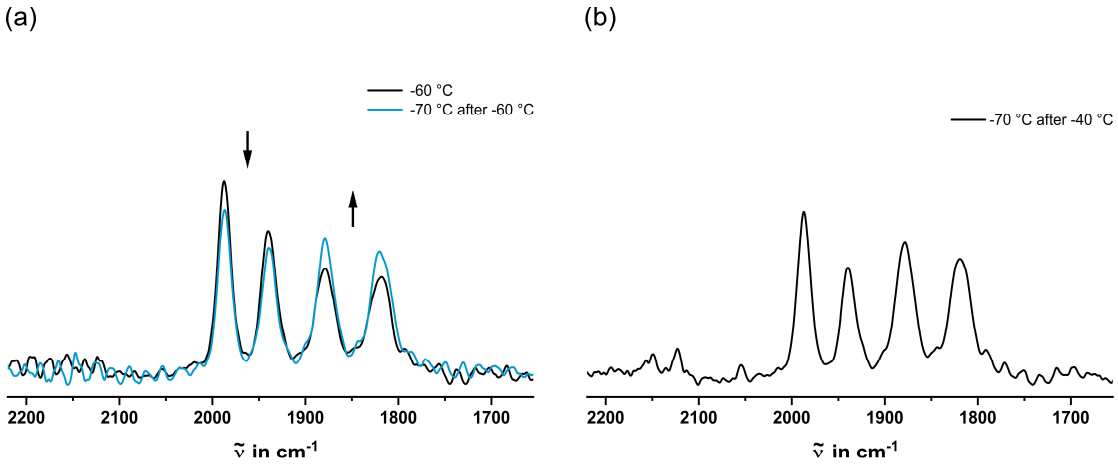


Figure S21. IR spectra of $\mathbf{3}^{+}$ in CH_2Cl_2 at (a) -70 after warming to -60 °C; (b) -70 after warming to -40 °C.

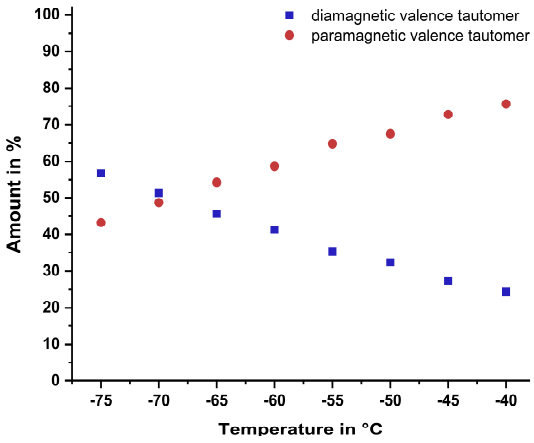


Figure S22. Amounts of the distinct valence tautomers of **3**$^{+}$ between -70 and -40 °C.

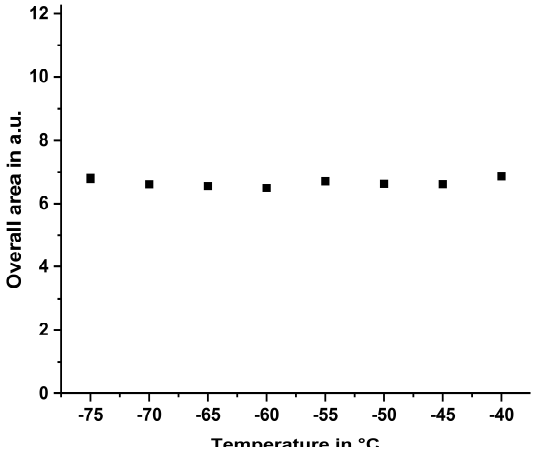


Figure S23. Total area of all carbonyl bands of complex **3**$^{+}$ within the temperature range from -70 to -40 °C.

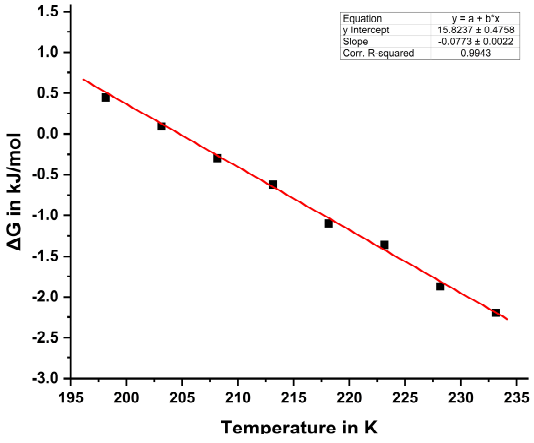


Figure S24. Plot of Δ*G* against *T* for **3**$^{+}$ with a linear regression line.

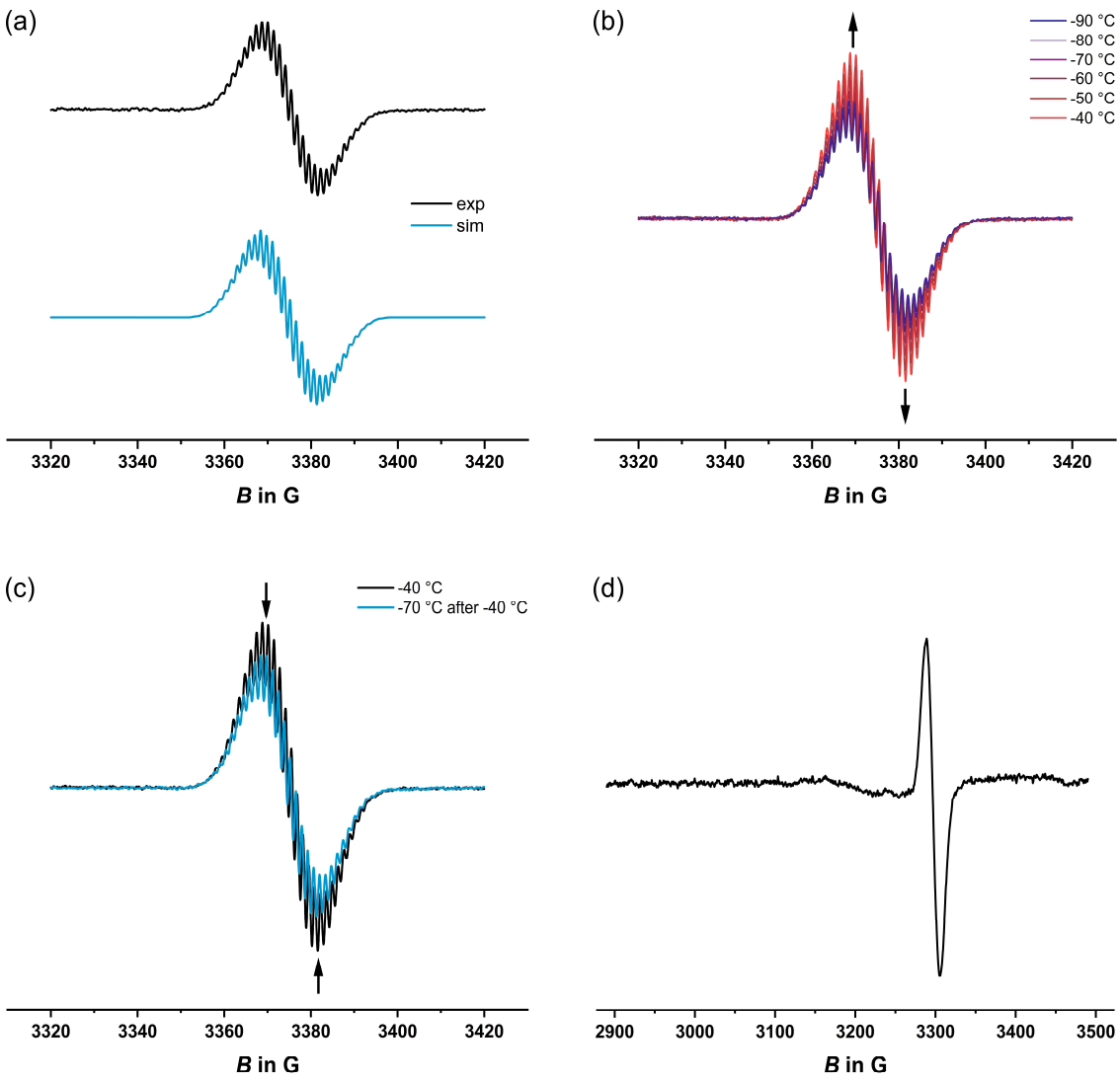


Figure S25. (a) EPR spectrum of $\mathbf{1}^{+}$ in CH_2Cl_2 at -70 °C (black) and corresponding simulation (blue). (b) EPR spectra of $\mathbf{1}^{+}$ in CH_2Cl_2 at temperatures between -90 and -40 °C. (c) EPR spectrum of $\mathbf{1}^{+}$ at -70 after warming to -40 °C. (d) EPR spectrum of $\mathbf{1}^{+}$ in frozen CH_2Cl_2 at 77 K.

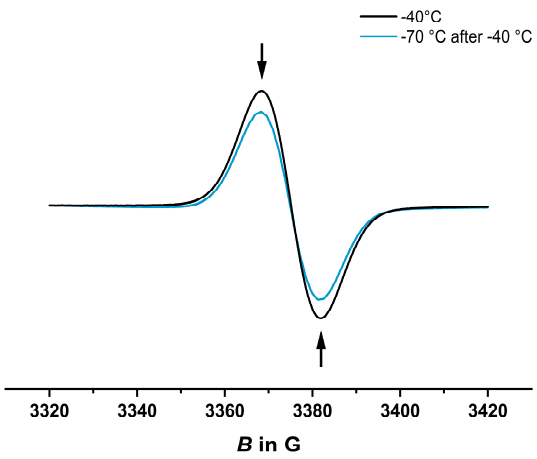


Figure S26. EPR spectra of $\mathbf{3}^{+}$ in CH_2Cl_2 at -40 °C (black) and at -70 after warming to -40 °C (blue).

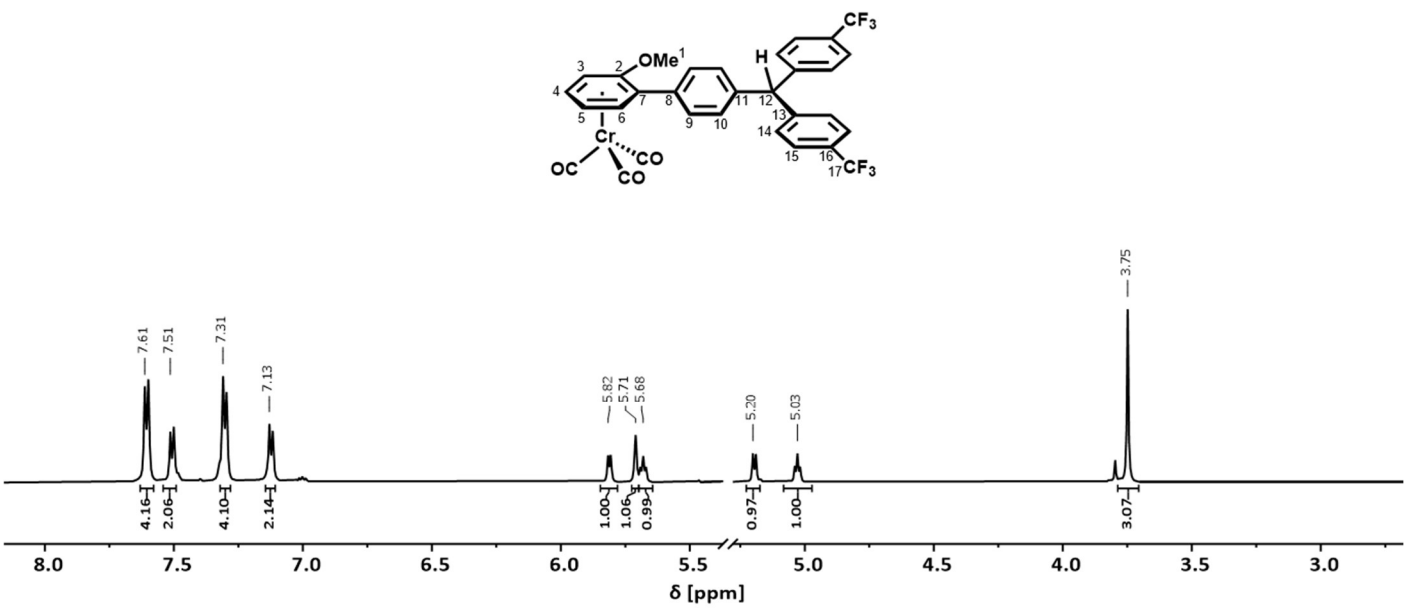


Figure S27. ^{1}H-NMR spectrum of complex **1-H** (600 MHz, CD_2Cl_2).

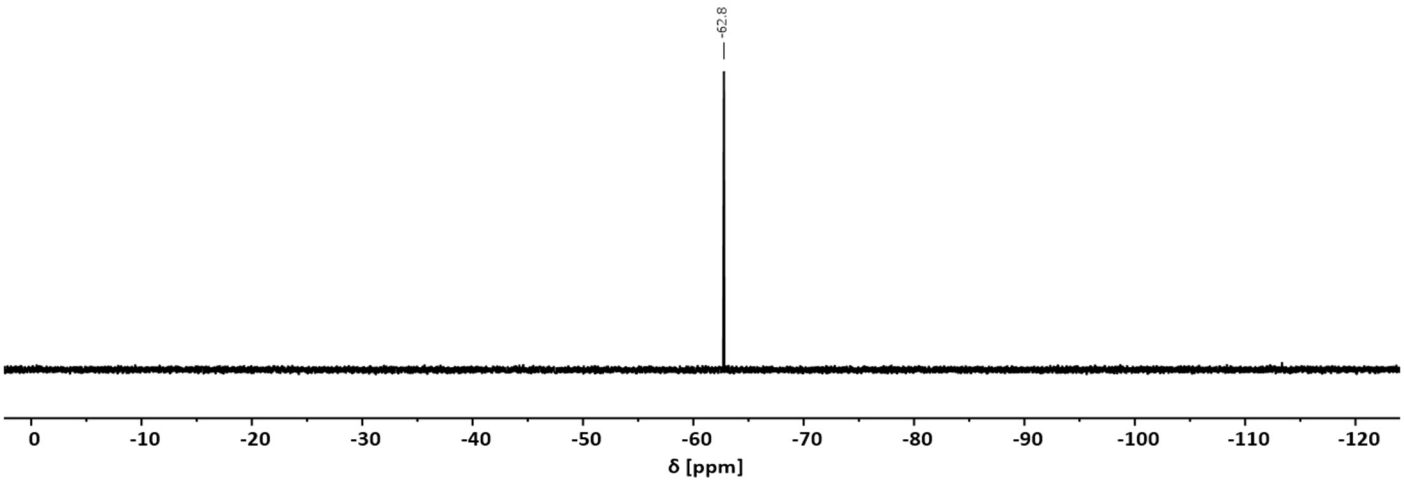


Figure S28. ^{19}F{^{1}H}-NMR spectrum of complex **1-H** (376 MHz, CD_2Cl_2).

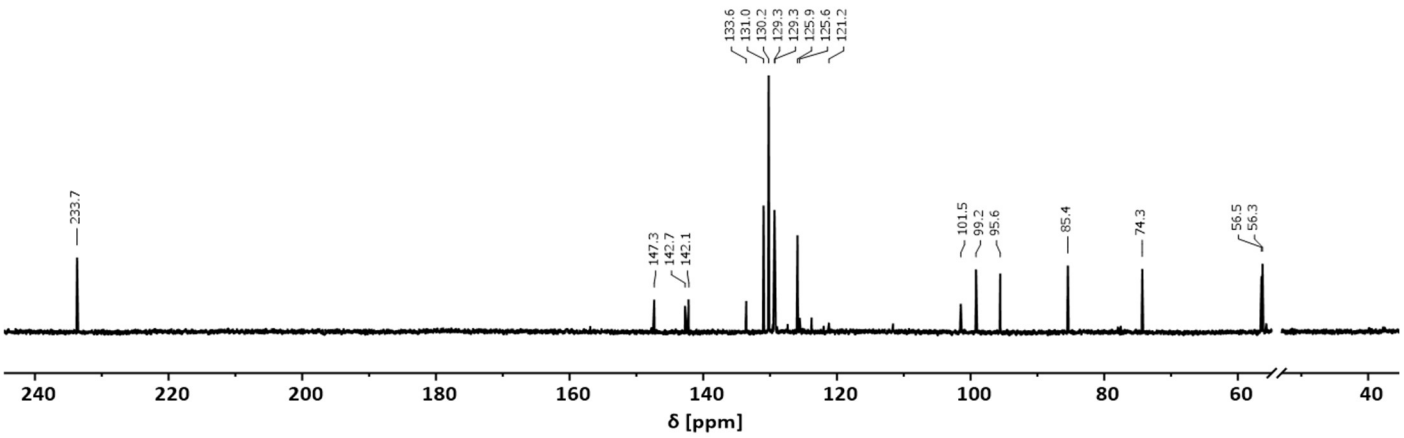


Figure S29. ^{13}C{^{1}H}-NMR spectrum of complex **1-H** (151 MHz, CD_2Cl_2).

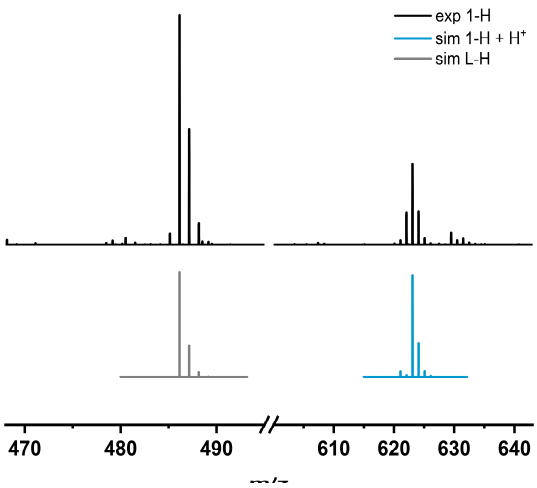


Figure S30. Experimental (black) and simulated (**1-H** +H⁺ blue, **L-H** grey) mass spectrum of complex **1-H**.

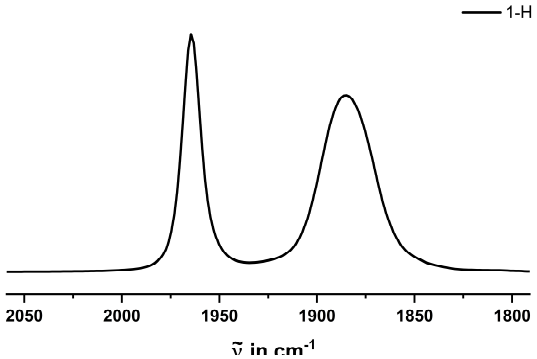


Figure S31. Carbonyl-region of the IR spectrum of complex **1-H** in CH_2Cl_2.

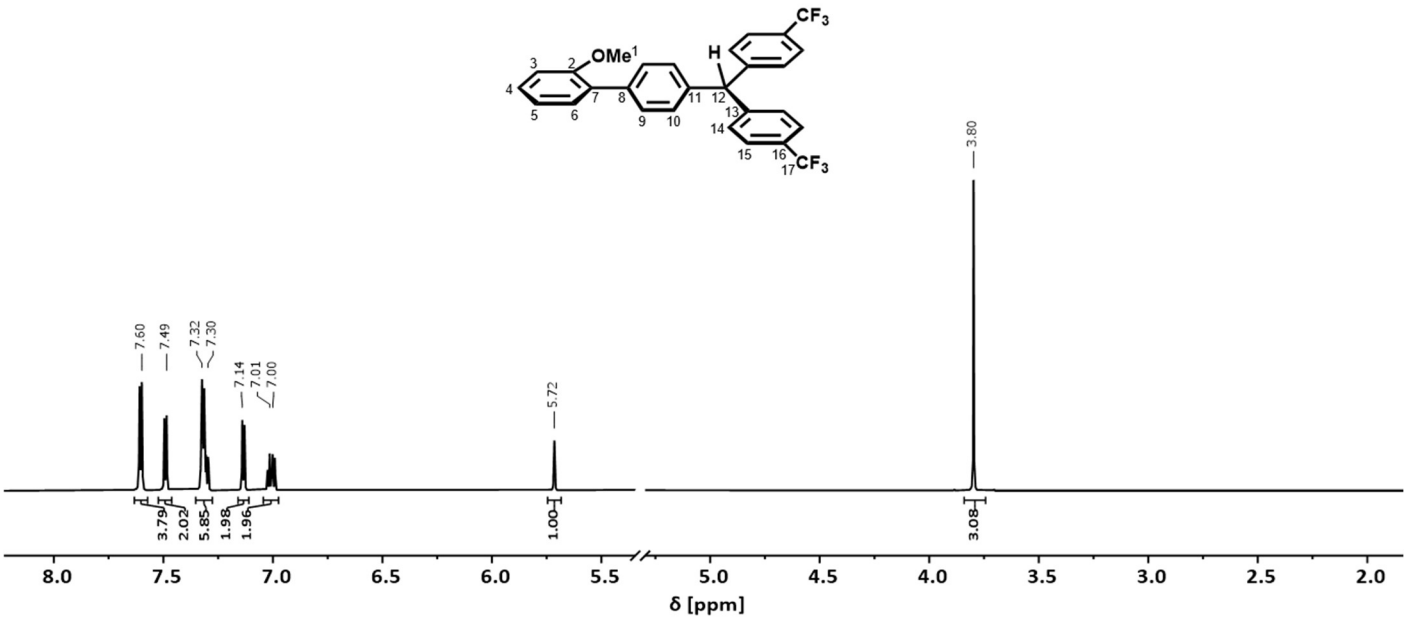


Figure S32. ^{1}H-NMR spectrum of **L-H** (800 MHz, CD_2Cl_2).

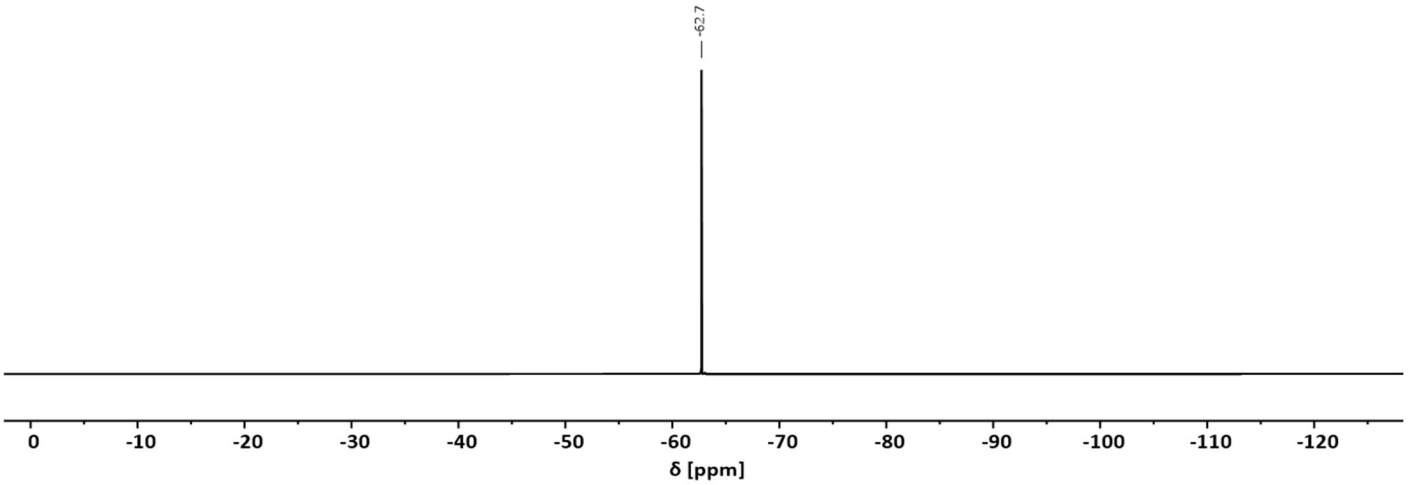


Figure S33. $^{19}F\{^{1}H\}$-NMR spectrum of **L-H** (752 MHz, CD_2Cl_2).

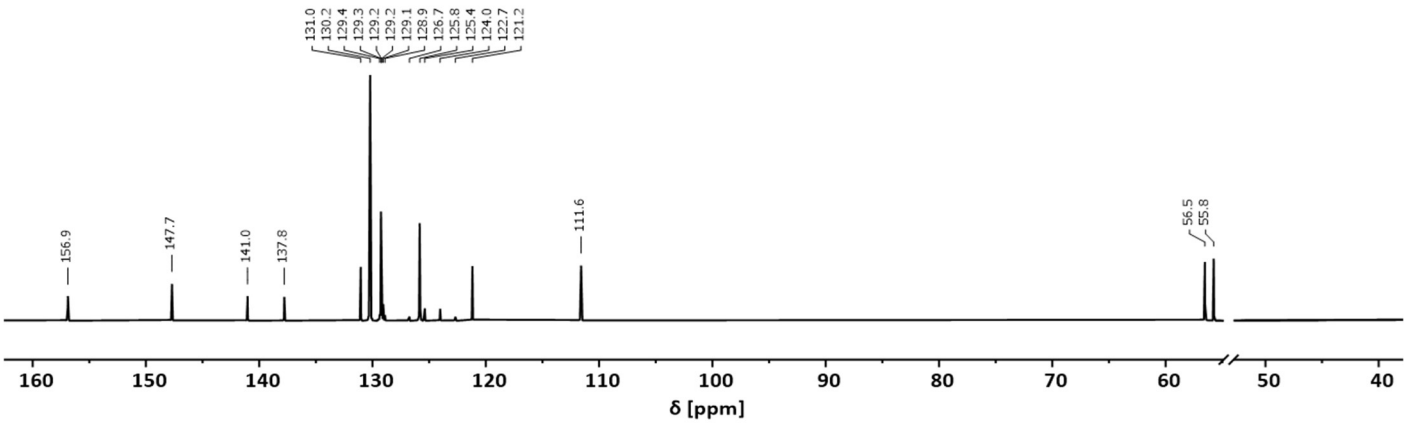


Figure S34. $^{13}C\{^{1}H\}$-NMR spectrum of **L-H** (202 MHz, CD_2Cl_2).

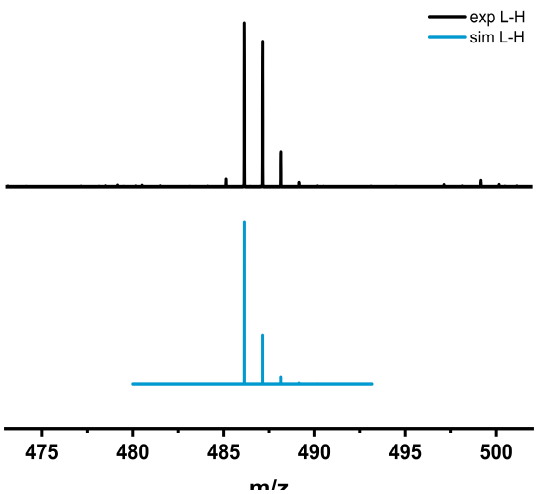


Figure S35. Experimental (black) and simulated (blue) mass spectrum of **L-H**.

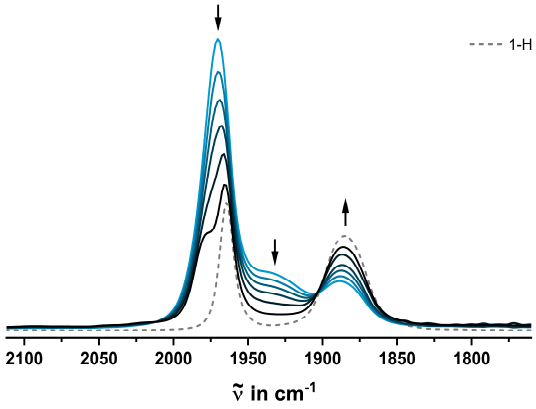


Figure S36. IR spectra recorded during decomposition of $\mathbf{1}^{+}$ at r.t. The grey broken line represents the IR spectrum of complex **1-H**.

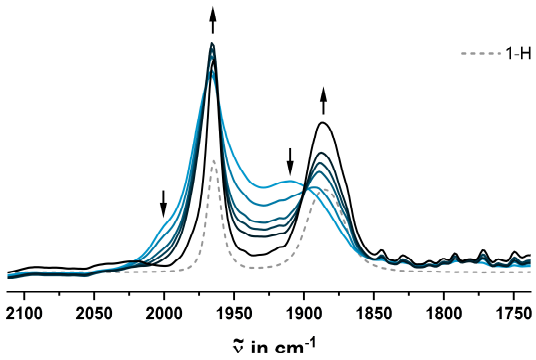


Figure S37. IR spectra recorded during decomposition of $\mathbf{2}^{+}$ at r.t. The grey broken line represents the IR spectrum of complex **1-H**.

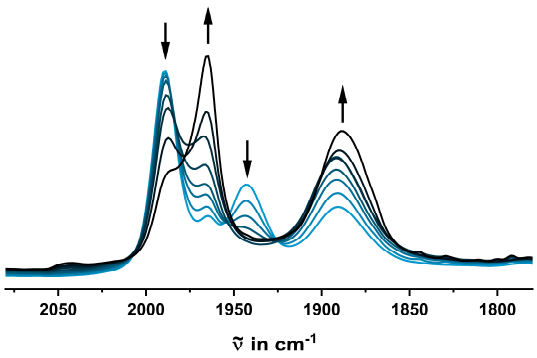


Figure S38. IR spectra recorded during decomposition of $\mathbf{3}^{+}$ at r.t.

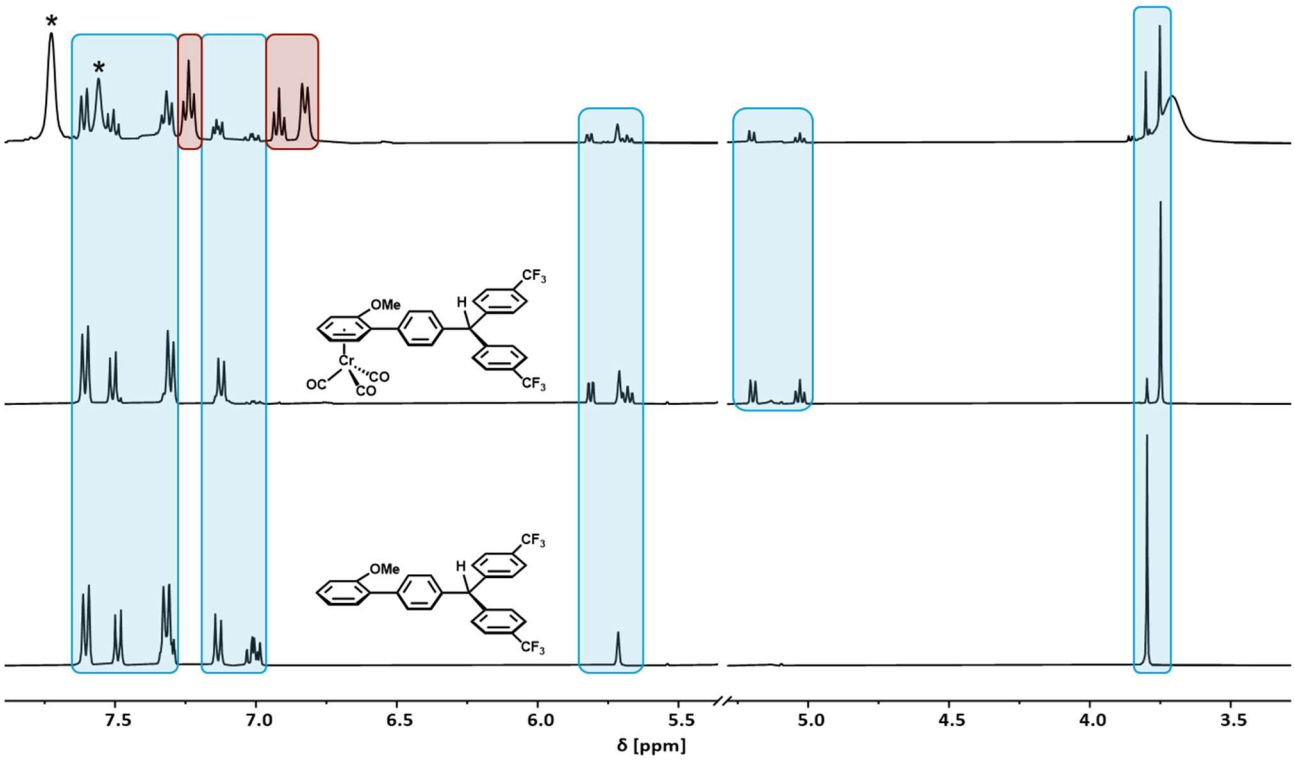


Figure S39. ^{1}H-NMR spectra of **2**$^{+}$ (top, 12 h after addition of Brookhart's acid at r.t.) and its decomposition products **1-H** (middle) and **L-H** (bottom) (400 MHz, CD_2Cl_2). $[BAr^{F_{24}}]^-$ signals are marked with asterisks. The signals marked in red could be assigned to phenol.

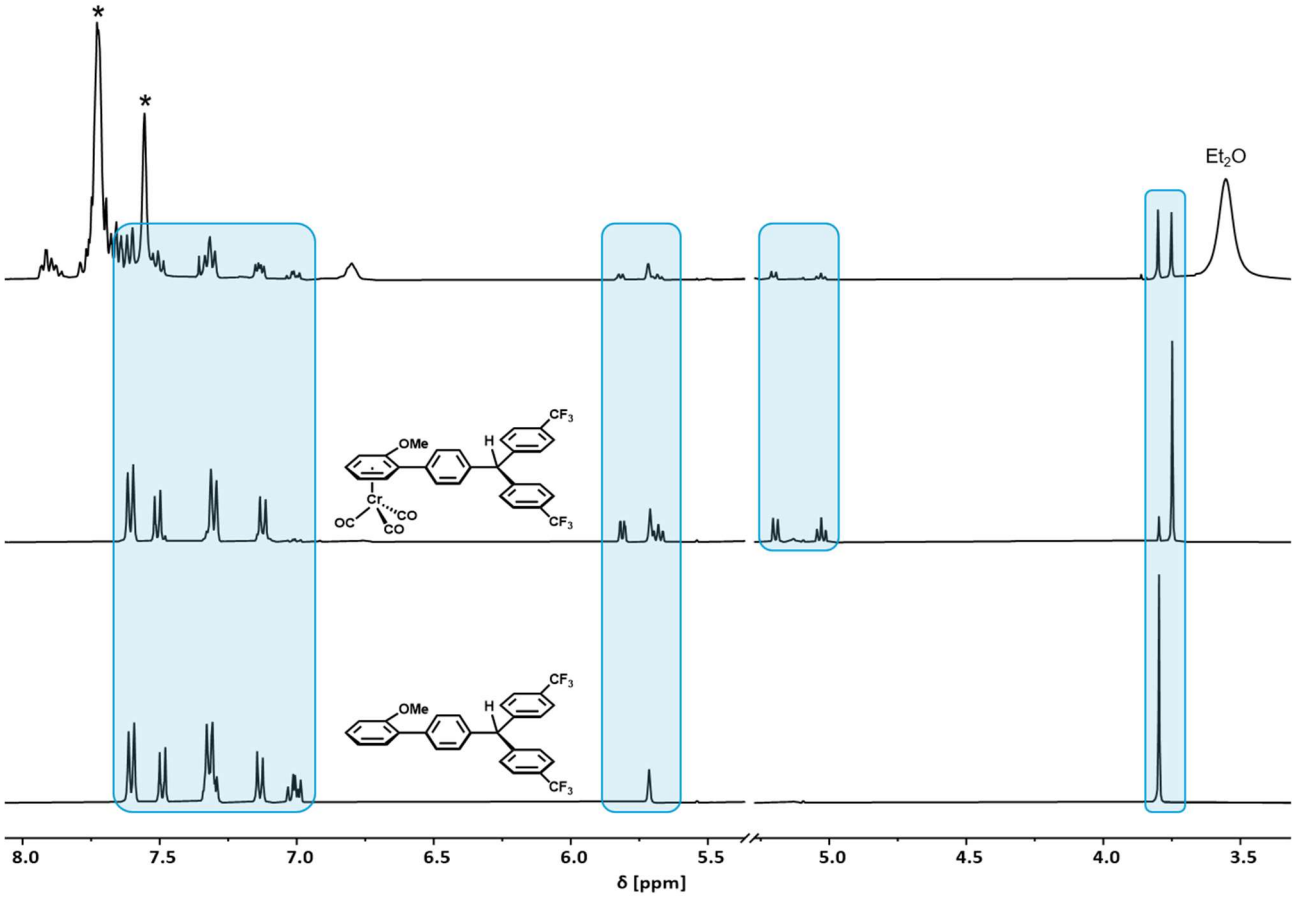


Figure S40. ^{1}H-NMR spectra of **2**$^{+}$ (top, 12 h after addition of Brookhart's acid at r.t.) and its decomposition products **1-H** (middle) and **L-H** (bottom) (400 MHz, CD_2Cl_2). $[BAr^{F_{24}}]^-$ signals are marked with asterisks.

Table S3. Crystal data and structure refinement for complex **1-H**.

Empirical formula	$C_{31}H_{20}CrF_6O_4$
Formula weight	622.47
Temperature / K	100
Crystal system	monoclinic
Space group	$P2_1/n$
a / Å	17.2787(10)
b / Å	7.6071(6)
c / Å	20.5128(12)
α / °	90
β / °	95.142(5)
γ / °	90
Volume / Å^3	2685.4(3)
Z	4
ρ_{calc}g / cm^3	1.540
μ / mm^{-1}	4.216
F(000)	1264.0
Crystal size / mm^3	0.17 × 0.068 × 0.015
Radiation	Cu Kα (λ = 1.54186)
2Θ range for data collection / °	6.412 to 132.054
Index ranges	$-20 \le h \le 20$, $-8 \le k \le 7$, $-24 \le l \le 19$
Reflections collected	12293
Independent reflections	4489 [R_{int} = 0.1260, R_{sigma} = 0.1315]
Data/restraints/parameters	4489/78/437
Goodness-of-fit on F^2	1.189
Final R indexes [$I \ge 2\sigma$ (I)]	R_1 = 0.1280, wR_2 = 0.3053
Final R indexes [all data]	R_1 = 0.2236, wR_2 = 0.3873
Largest diff. peak/hole / e Å^{-3}	1.45/-0.93

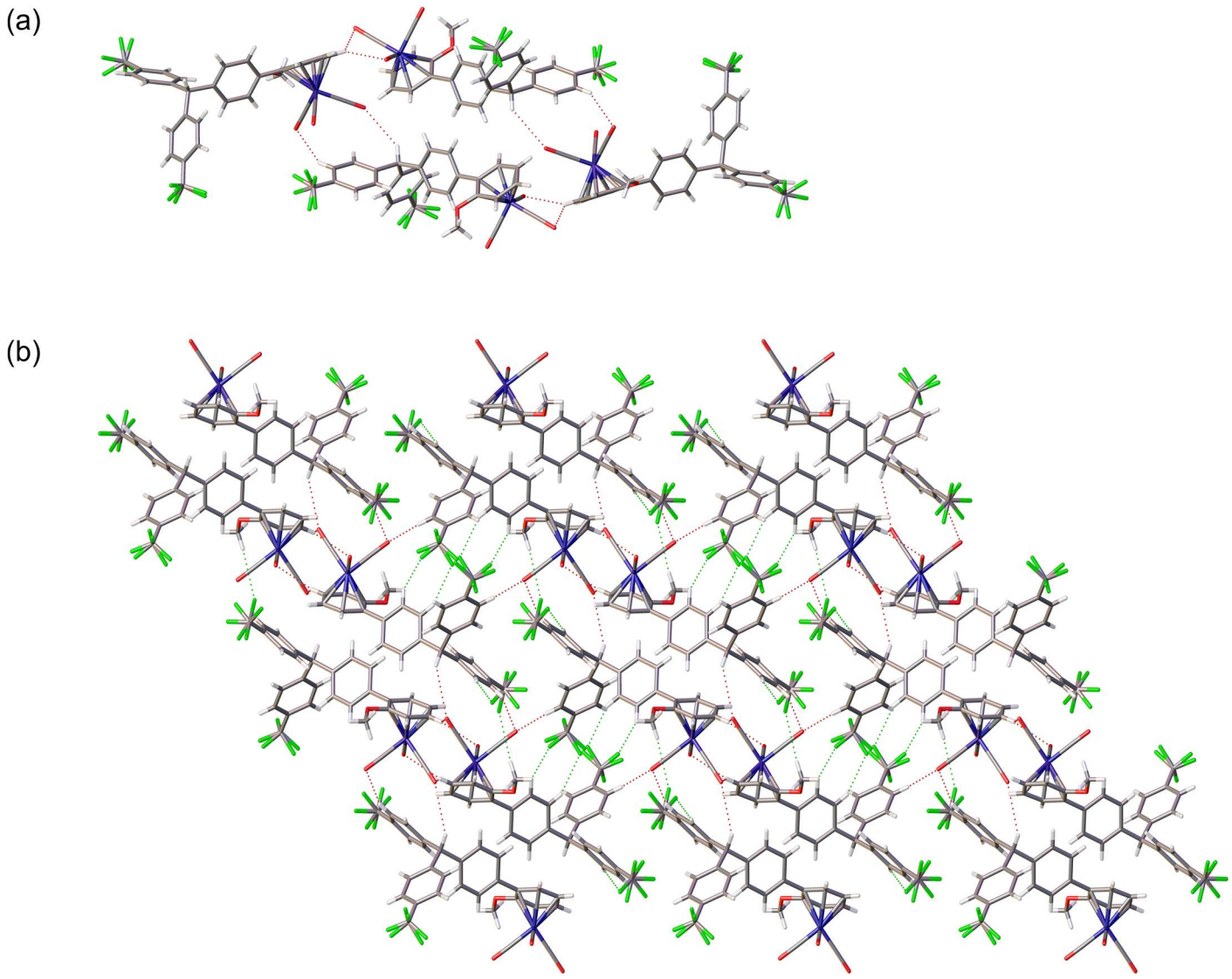


Figure S41. (a) Packing of two R_P and S_P enantiomers each of **1-H** within the unit cell. (b) Packing of the units; view along the *b* axis. Short contacts are indicated by red broken lines.

Table S4. Crystal data and structure refinement for **L-H**.

Empirical formula	$C_{28}H_{20}F_6O_{1.04}$
Formula weight	487.08
Temperature / K	100
Crystal system	orthorhombic
Space group	*Pbca*
a / Å	9.6538(4)
b / Å	18.3824(6)
c / Å	25.4401(7)
α / °	90
β / °	90
γ / °	90
Volume / Å^3	4514.6(3)
Z	8
ρ_{calc}g / cm^3	1.433
μ / mm^{-1}	0.120
F(000)	2003.0
Crystal size / mm^3	0.3 × 0.25 × 0.2
Radiation	Mo Kα (λ = 0.71073)
2Θ range for data collection / °	5.028 to 55.118
Index ranges	$-12 \le h \le 12$, $-23 \le k \le 22$, $-33 \le l \le 30$
Reflections collected	17345
Independent reflections	5176 [R_{int} = 0.0228, R_{sigma} = 0.0206]
Data/restraints/parameters	5176/62/375
Goodness-of-fit on F^2	1.103
Final *R* indexes [$I \ge 2\sigma(I)$]	R_1 = 0.0415, wR_2 = 0.0905
Final *R* indexes [all data]	R_1 = 0.0611, wR_2 = 0.1088
Largest diff. peak/hole / e Å^{-3}	0.29/-0.23

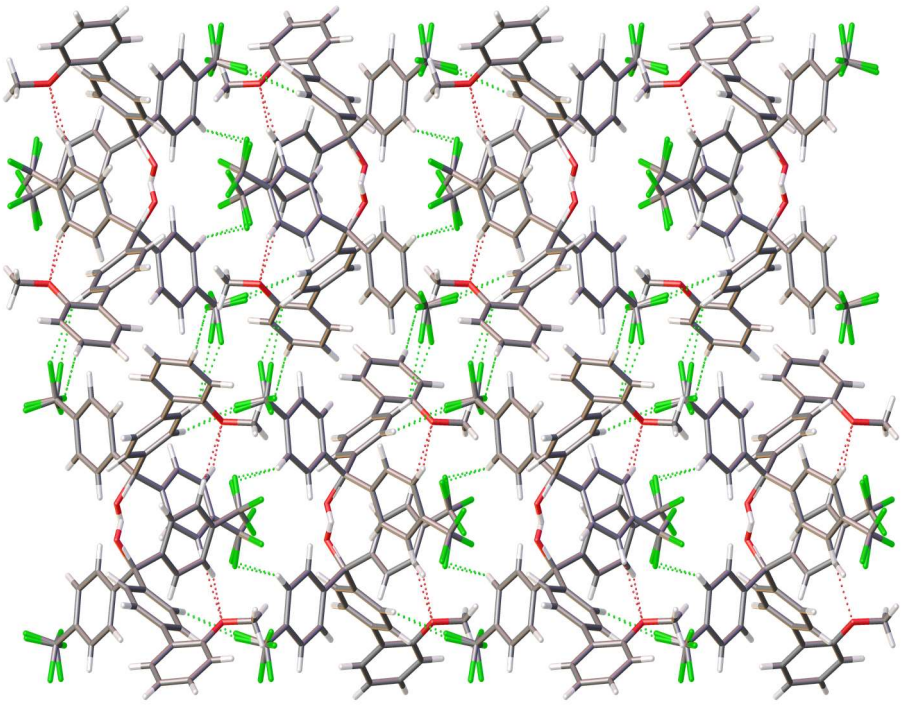


Figure S42. Packing of **L-H**; view along the *a* axis.

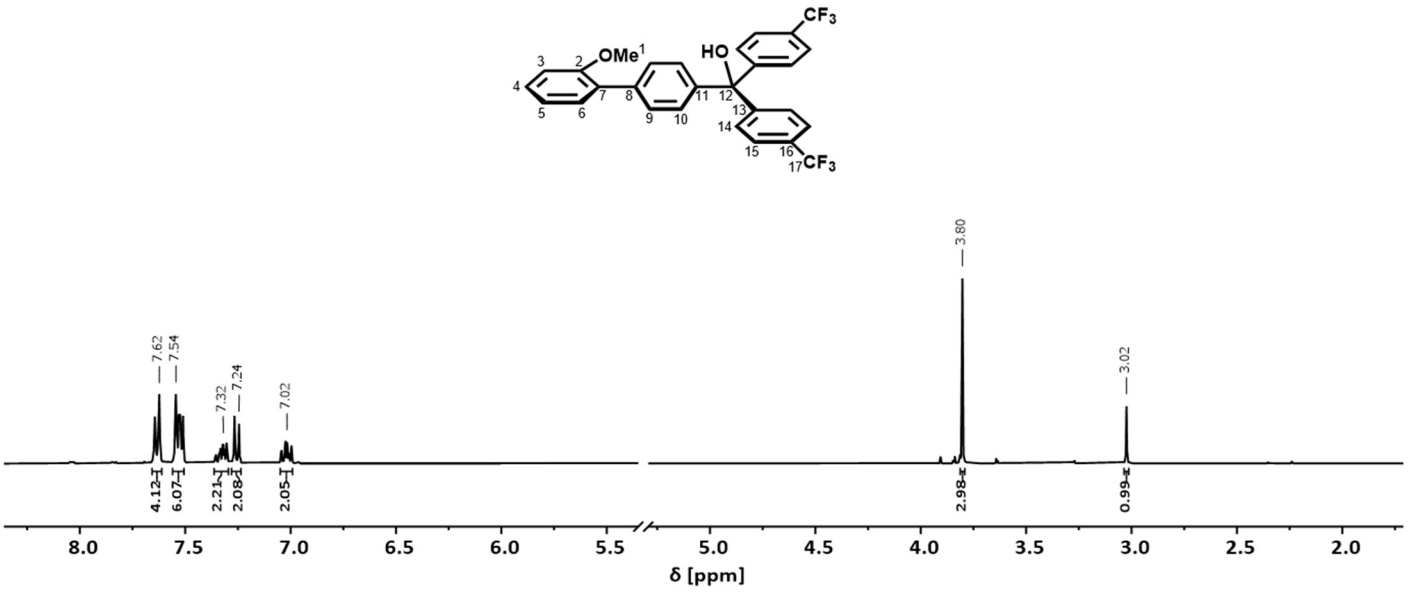


Figure S43. ^{1}H-NMR spectrum of **L-OH** (400 MHz, CD_2Cl_2).

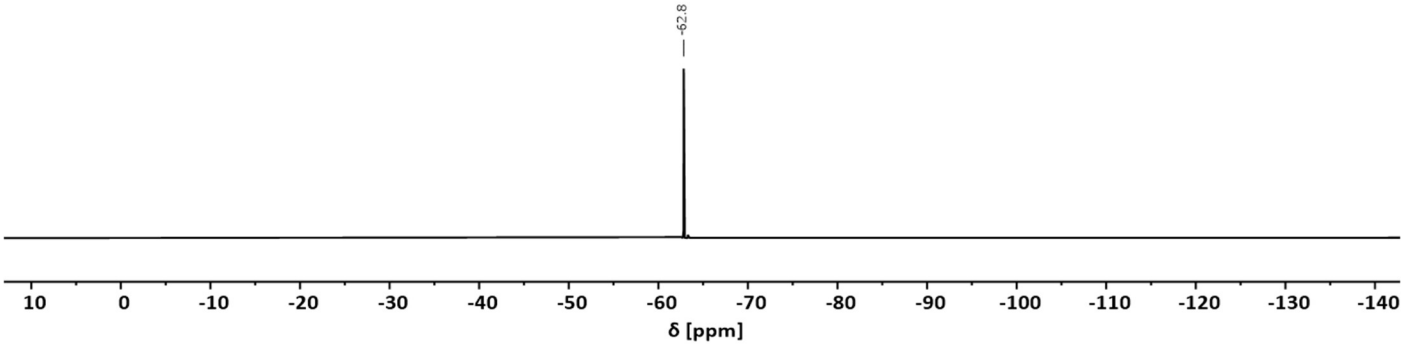


Figure S44. ^{19}F{^{1}H}-NMR spectrum of **L-OH** (376 MHz, CD_2Cl_2).

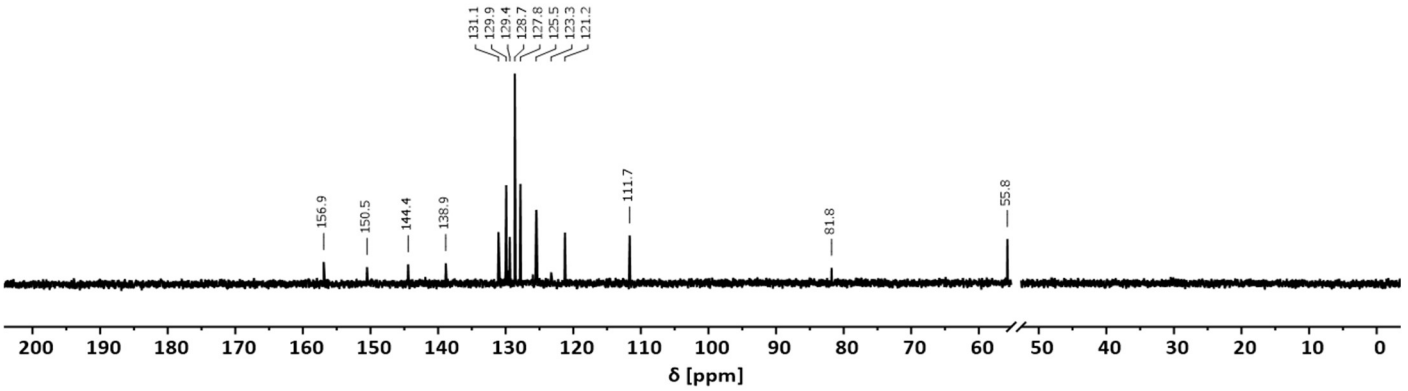


Figure S45. ^{13}C{^{1}H}-NMR spectrum of **L-OH** (101 MHz, CD_2Cl_2).

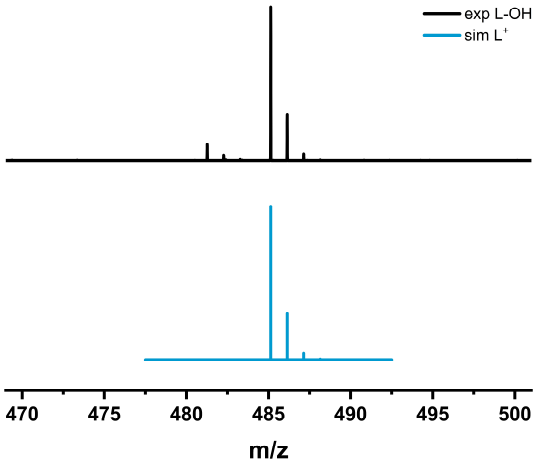


Figure S46. Experimental (black) and simulated (blue) mass spectrum of **L-OH**.